Stopping of ions with extended charge distribution in dense matter

C. Deutsch and G. Maynard
Laboratoire de Physique des Gaz et des Plasmas, Université Paris–Sud, 91405 Orsay CEDEX, France
(Received 6 March 1989)

The stopping of partially stripped ions by a partially ionized target is investigated for the case of a projectile with an extended electronic core. Long-ranged contributions to energy loss are evaluated within an impact-parameter theoretical framework. Quantities correcting the standard pointlike results are given in analytical form with the aid of a Thomas-Fermi-like effective interaction. They can be substantial for moderate projectile ionicity and for velocities relevant for inertial confinement fusion driven by intense ion beams. As a rule, the stopping quantities pertaining to projectiles with extended core taken into account lie above those computed for their pointlike homologs.

I. INTRODUCTION

The purpose of this work is to explore in a quantitative way the stopping of the extended charge distribution brought by a nonrelativisitic and partially stripped ion projectile in dense and moderately hot matter. The latter is taken as a collection of so weakly interacting partially ionized atoms that the mean excitation energy involved in the bound-state portion of the Bethe stopping formula retains its isolated ion value. A previous and detailed study shows that the corresponding target temperature should thus remain below 10 eV.[1]

The basic motivation of our efforts lies in the possibility afforded by intense ion beams to successfully compress, up to ignition, hollow pellets containing the thermonuclear D+T fuel contained within their interior.[2] To achieve this goal, one has to focus on the pellet target, heavy ions transported at the smallest ionicity, e.g., $_{92}U^{+}$ or Bi^{+} with an energy $\sim$ 50 MeV/nucleon. This particular situation led us naturally to question the usual pointlike projectile assumption used in nearly every stopping formulation.

As far as we know, there is only scarce attention in the literature paid to the dynamical inferences of the projectile core electron on its stopping performance in a given medium.

Nevertheless, certain attention has already been given to the transfer of energy between electrons bound to the projectile and those attached to the target ion. This point has been discussed through form factors of inelastic processes in Fourier-transformed space.[3] Here we shall explore the so-called extended projectile core effect (EPCE) in direct space within the standard impact formalism, by modeling the incoming ion electromagnetic structure as well as that of the target ion, through a Thomas-Fermi description making use of pseudopotentials (Sec. II). The latter are introduced in the impact formalism (Sec. III) and yield analytic Bethe-like stopping expressions including projectile, as well as target-ion, extended charge distributions. The present work is mostly restricted to the distant impact contribution. The stability of the lower parameter cutoff involved in the impact calculation is then asserted in Sec. IV. The results (Sec. V) are then discussed in relation to their relevance to the stopping of energetic ions in thermonuclear targets. The significance of a low ionicity for at least one partner in a given projectile-target pair in connection with the resulting enhanced stopping is also stressed.

II. IONS WITH EXTENDED CHARGE DISTRIBUTION

Radial distributions for the remaining electrons bound to the incoming ion projectile, as well as for those pertaining to the partially stripped target ion, are derived within a Thomas-Fermi-like theoretical framework.

The projectile charge distribution is worked out analytically through the so-called Green-Sellin-Zachor (GSZ) parametrization.[4,5] Recently, we have thoroughly investigated target temperature effects on stopping of energetic incoming ions taken as pointlike.[1] As a consequence, we shall restrict our attention here to temperatures, $k_B T \leq 10$ eV, in order to neglect any plasma effects on the bound-state target stopping. Then, we focus our attention on isolated and partially stripped target ions.

The Coulomb interaction between an electron bound to a given nucleus in target and the extended projectile charge distribution is conveniently taken in the GSZ formulation[4,5]

$$V(r)=[N-Z-N\Omega_E(r)]r^{-1}\ \text{a.u.}\ , \tag{1}$$

where

$$\Omega_E(r)=\frac{A\exp[-(1+\alpha)\xi r]}{(1+\alpha)^2} + \frac{B\exp[-(1+\beta)\xi r]}{(1+\beta)^2}+C\exp(-r\xi)\ , \tag{2}$$

$$A=\left[\frac{1}{H}-\frac{1}{H^2}-\frac{2H-1-H^{-2}}{1+\beta^2}\right]D^{-1},$$
$$B=\left[\frac{2H-1-H^{-2}}{(1+\alpha)^2}-\frac{1}{H}+\frac{1}{H^2}\right]D^{-1},$$
$$C=H^{-2},$$
$$D=(1+\alpha)^{-2}-(1+\beta)^{-2} \tag{3}$$

for a projectile with atomic number Z and N core electrons. It should be noticed that in Eq. (1), the $N-1$ given in Refs. 4 and 5 has been modified into N to comply with the fact that the projectile potential interacts with the target and not with a projectile core electron.

Parameters H, α, and β are taken from Ref. 4 while $\xi=\xi_0+\xi_1(Z-N)$ with ξ_0 and ξ_1 specified for a given (N,Z) in Ref. 5. Equation (2) obtains as a long-range expansion ($r\gg a_0$, Bohr radius) of the compact and Thomas-Fermi-like GSZ effective interaction,

$$\Omega_E(r)=[H(e^{\xi r}-1)+1]^{-1} \tag{4}$$

valid for any r positive value. Finally, the radial distributions themselves are obtained through the Poisson equation, in terms of the second spatial derivative of Eq. (2) as

$$\rho(r)=\frac{N}{4\pi r}\Omega_E''(r)$$
$$=\frac{NH\xi^2}{4\pi r}(Ae^{-(1+\alpha)\xi r}+Be^{-(1+\beta)\xi r}+Ce^{-\xi r}). \tag{5}$$

They are normalized with

$$\int_0^\infty dr\,4\pi r^2\rho(r)=N.$$

Typical parameters featuring a few ionized species are listed in Table I. They will be extensively used in the following.

Equation (2) and Table I enable us to treat quantitatively the ion core distribution of electron charge on a symmetric footing for the projectile and the partially ionized target. It should be kept in mind that we restrict our present considerations to an improved Thomas-Fermi-like approximation with melted shell structures. We therefore expect the present formalism to be mostly appropriate at evidencing average extended charge effect in the forthcoming stopping calculation devoted to the large impact-parameter contribution.

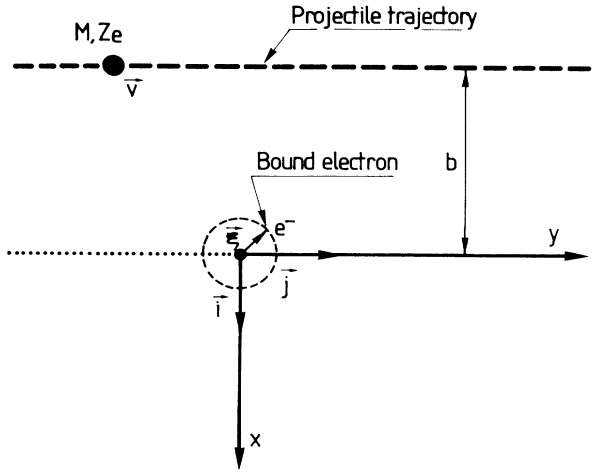

FIG. 1. Schematic of the ion projectile with an extended charge distribution interacting with electrons bound to the partially stripped target. The impact parameter b is assumed larger than the average projectile distribution diameter.

III. CLASSICAL IMPACT FORMALISM FOR ION STOPPING

A. General theory

The modified Coulomb-like interaction (1) thus allows us to proceed in a systematic way with the analytic and impact formalism for the distant contribution to ion stopping in a partially ionized plasma. The projectile diameter must then remain far smaller than the average impact distance (see Fig. 1). We thus restrict to the so-called distant stopping contribution. Working within a classical conceptual framework rigorously equivalent to the standard quantum-mechanical one, one is led to picture a target bound electron as a harmonic oscillator (HO) experiencing a force $\mathbf{f}(t,b)$ so that its displacement vector $\xi(t)$ fulfills

$$\ddot{\xi}(t)+\omega^2\xi(t)=\frac{\mathbf{f}(t,b)}{m_e}, \tag{6}$$

TABLE I. Parameters for the ion GSZ pseudopotential [Eq. (2)].

Species	Z	N	H	ξ	α	β
C^{4+}	6	2	0.892 13	1.2996	1.514 16	1.038 61
Al^{8+}	13	5	1.194 96	4.970 20	2.354 55	1.0088
Al^{3+}	13	10	1.211 28	3.146 50	2.4504	1.009 00
Al^{11}	13	2	0.845 845	16.9206	1.629 026 4 4	1.018 40
Mo^{18+}	42	24	1.459 90	5.2618	3.086 69	1.054 78
Mo^{25+}	42	17	1.463 52	6.853 00	3.088 26	1.0548
Cs^{1+}	55	54	4.5315	1.1547	9.3021	1.721 85
Cs^{3+}	55	52	3.738 634	1.4562	7.572 614 5	1.058 565
Cs^{5}	55	50	3.092 74	1.8275	6.417 644	1.377 185
Xe^{24+}	54	30	1.298 04	6.5924	2.669 40	1.0255

with

$$\xi(t)=\mathrm{Re}\left[\frac{i}{m\omega}\int_{-\infty}^{t}dt'\mathbf{f}(t',b)e^{-i\omega(t-t')}\right] \tag{7}$$

and where m_e is the electron mass.

The target basic entity (ion or atom) is thus equivalent to F_ω oscillators with frequency ω. Actually, F_ω denotes the fraction of oscillators responding in the frequency range between ω and $\omega+d\omega$. It is equal to $g(\omega)d\omega$, where $g(\omega)$ is the differential oscillator strength normalized such that

$$\int_0^\infty g(\omega)d\omega=1 \ .$$

At time t, the target energy gain per electron can be written as

$$\frac{m}{2}(\ddot{\xi}^2+\omega^2\xi^2)=W_r(t,b)=\frac{1}{2m}\left|\int_{-\infty}^{t}\mathbf{f}(t',b)e^{i\omega t'}dt'\right|^2 . \tag{8}$$

The corresponding stopping power thus reads as

$$\left.\frac{dE}{dx}\right|_\omega=-2\pi nN'F_\omega\int_{a_\omega}^{\infty}db\ bW_r(\infty,b) \ , \tag{9}$$

with N' bound electrons per target ion of density n_i. a_ω denotes the minimum impact parameter fulfilling the dipole approximation.

As already stressed above, the target temperature is taken low enough ($k_B T_e \leq 10$ eV) that the isolated mean excitation energy does not get perturbed through collective or excitation plasma contribution. The target plasma is thus viewed as a collection of isolated and noninteracting ions. The geometry of the projectile–bound-electron interaction is depicted in Fig. 1. The condition $b>a_\omega$ entitles us to use the corresponding effective potential under the asymptotic form (2), a superposition of three Debye-like expressions. Now, we modify in a straightforward way the usual Coulomb treatment by replacing the electric field $-r/r^3$ with $-(r/r^3)(1+\xi r)e^{-\xi r}$ and similar terms pertaining to a statically screened Coulomb interaction.

Next, we concentrate our attention on the distant collision contribution with an impact parameter b (Fig. 1) larger than a_0. Upon introducing Eqs. (1), (2), and (3) into the standard impact formulation,[6–8] one gets the force acting on a target electron (V is the linear projectile velocity)

$$\begin{aligned}\mathbf{f}(t,b)=&\frac{e^2\{[b+\xi(t)]\mathbf{i}-[Vt-\xi_y(t)]\mathbf{j}\}}{\{[b+\xi_x(t)]^2+[Vt-\xi_y(t)]^2\}^{3/2}}\\&\times\left[(N-Z)-N\sum_{i=1}^{3}a_i\exp^{(-b_i\{[b+\xi_x(t)]^2+[Vt-\xi_y(t)]^2\}^{1/2})}\right.\\&\left.\times(1+b_i\{[b+\xi_x(t)]^2+[Vt-\xi_y(t)]^2\}^{1/2})\right]\equiv\mathbf{f}_0(t,b)+\Delta\mathbf{f}(t,b) \ ,\end{aligned} \tag{10}$$

pertaining to the geometry of Fig. 1. In this work we limit ourselves to $\mathbf{f}_0(t,b)$, and the ensuing Bohr-Bethe-Bloch term proportional to $(Z-N)^2$, which amounts to neglecting first-order corrections in $\xi(t)$, the displacement of target electron.

Equation (10) is finally explained with

$$\begin{aligned}&a_1=A(1+\alpha)^{-2}, \quad a_2=B(1+\beta)^{-2}, \quad a_3=C\\&b_1=(1+\alpha)\xi, \quad b_2=(1+\beta)\xi, \quad b_3=\xi \ .\end{aligned} \tag{11}$$

The last term on the right-hand side (r.h.s.) of Eq. (10) fulfills the requirement $\xi_{x,y}(b^2+V^2t^2)^{-1/2}\ll 1$. Recalling that a given (N,Z) pair specifies a given projectile species, one can write

$$\mathbf{f}_0(t,b)=e^2\frac{b\mathbf{i}-Vt\mathbf{j}}{(b^2+V^2t^2)^{3/2}}\left[(N-Z)-N\sum_{i=1}^{3}a_i e^{-b_i(b^2+V^2t^2)^{1/2}}[1+b_i(b^2+V^2t^2)^{1/2}]\right] , \tag{12}$$

and

$$\begin{aligned}\Delta f(t,b)=&e^2\{[(-2b^2+V^2t^2)\xi_x+3bV\xi_y]\mathbf{i}+[(b^2-2V^2t^2)\xi_y+3bV\xi_x]\mathbf{j}\}\\&\times(b^2+V^2t^2)^{5/2}\left[(N-Z)-N\sum_{i=1}^{3}a_i e^{-b_i(b^2+V^2t^2)^{1/2}}[1+b_i(b^2+V^2t^2)^{1/2}]\right]\\&+e^2\frac{b\mathbf{i}-Vt\mathbf{j}}{(b^2+V^2t^2)^{3/2}}(b\xi_x-Vt\xi_y)\left[\sum_{i=1}^{3}a_i b_i^2 e^{-b_i(b^2+V^2t^2)^{1/2}}\right] .\end{aligned} \tag{13}$$

Equation (13) is derived through the replacements

$$e^{-b_i[(b+\xi_x)^2+(Vt-\xi_y)^2]^{1/2}} \simeq e^{-b_i(b^2+V^2t^2)^{1/2}}\left[1-\frac{b_i(b\xi_x-Vt\xi_y)}{(b^2+V^2t^2)^{1/2}}\right],$$

$$[(b+\xi_x)^2+(Vt-\xi_y)^2]^{1/2} \simeq (b^2+V^2t^2)^{1/2}+\frac{b\xi_x-Vt\xi_y}{(b^2+V^2t^2)^{1/2}} .$$

B. Analytic calculation

Setting $N=0$ yields the pointlike treatment due to Jackson and McCarthy.[7] In this work, we pay thorough attention to the terms proportional to the Z^2 term. The corresponding ω-indexed stopping power thus reads as

$$\left.\frac{dE}{dx}\right|_{\omega}^{0} = -2\pi n_i N' F_\omega \int_{a_\omega}^{\infty} db\, b(W_1+W_2) , \tag{14}$$

where

$$2mW_1 = \left| \int_{-\infty}^{\infty} dt \frac{be^{i\omega t}}{(b^2+v^2t^2)^{3/2}} \left[(N-Z) - N\sum_{i=1}^{3} a_i e^{-b_i(b^2+v^2t^2)^{1/2}} [1+b_i(b^2+v^2t^2)^{1/2}] \right] \right|^2 \tag{15}$$

and

$$2mW_2 = \left| \int_{-\omega}^{\infty} dt \frac{(-vt)e^{i\omega t}}{(b^2+v^2t^2)^{1/2}} \left[(N-Z) - N\sum_{i=1}^{3} a_i e^{-b_i(b^2+v^2t^2)^{1/2}} [1+b_i(b^2+v^2t^2)^{1/2}] \right] \right|^2 . \tag{16}$$

W_1 is easily evaluated analytically through the quadratures ($x=vt/b$) (Ref. 9)

$$\left| \int_{-\infty}^{\infty} \frac{dtbe^{i\omega t}}{(b^2+v^2t^2)^{3/2}} \right|^2 = \frac{4}{b^2v^2} K_1^2\left[\frac{\omega b}{v}\right]\left[\frac{\omega b}{v}\right]^2 , \tag{17}$$

$$\left| b\int_{-\infty}^{\infty} dt \frac{e^{i\omega t - b_i b(1+x^2)^{1/2}}}{(b^2+v^2t^2)^{3/2}} [1+bb_i(1+x^2)^{1/2}] \right|^2 = \frac{4}{b^2v^2}\left[\frac{\omega^2b^2}{v^2}+b^2b_i^2\right] K_1^2\left[\left[\frac{\omega^2b^2}{v^2}+b^2b_i^2\right]^{1/2}\right] , \tag{18}$$

with $K_1(z)$ the modified Bessel function of the second kind of order 1. It can be written with

$$\begin{aligned} 2mW_1 \equiv \frac{4e^4}{b^2v^2} \Big[& (N-Z)^2 K_1^2(z) z^2 + \sum_{i=1}^{3} N^2 a_i^2 (z^2+b^2b_i^2) K_1^2((z^2+b^2b_i^2)^{1/2}) \\ & -2(N-Z)N\sum_{i=1}^{3} a_i K_1(z)(z^2+b^2b_i^2)^{1/2} K_1((z^2+b^2b_i^2)^{1/2}) \\ & +2N^2 \Big[a_1(z^2+b^2b_1^2)^{1/2} K_1((z^2+b^2b_1^2)^{1/2}) a_2(z^2+b^2b_2^2)^{1/2} K_1((z^2+b^2b_2^2)^{1/2}) \\ & \quad + a_3(z^2+b^2b_3^2)^{1/2} K_1((z^2+b^2b_3^2)^{1/2}) \\ & \quad + a_2(z^2+b^2b_2^2)^{1/2} K_1((z^2+b^2b_2^2)^{1/2}) \\ & \quad \times a_3(z^2+b^2b_3^2)^{1/2} K_1((z^2+b^2b_3^2)^{1/2}) \Big] \Big] , \end{aligned} \tag{19}$$

where $z=\omega b/V$.

The corresponding contribution to the r.h.s. of Eq. (14) is further analytically expressed in terms of the quadratures

$$\int_{a_\omega}^{\infty} dbb\, K_1^2(\alpha b) = \frac{a_\omega^2}{2}\left[K_0^2(\alpha a_\omega) - K_1^2(\alpha a_\omega) + \frac{2K_0(\alpha a_\omega)K_1(\alpha a_\omega)}{\alpha a_\omega} \right] , \tag{20}$$

$$\int_{a_\omega}^{\infty} dbb\, K_1(\alpha_1 b) K_1(\alpha_2 b) = \frac{1}{\alpha_1^2-\alpha_2^2}[+\alpha_1 a_\omega K_0(\alpha_1 a_\omega) K_1(\alpha_2 a_\omega) - \alpha_2 a_\omega K_0(\alpha_2 a_\omega) K_1(\alpha_1 \omega)] . \tag{21}$$

$K_0(x)$ is the modified Bessel function of the second kind of orders 0.

Similarly, Eq. (16) is processed analytically with[9]

$$\left[\int_0^{\infty} dx \frac{x\sin(zx)}{(1+x^2)^{3/2}} \right]^2 = K_0^2(z) z^2 , \tag{22}$$

$$\left[\int_0^\infty dx \frac{x\sin(zx)}{(1+x^2)^{3/2}} e^{-bb_i(1+x^2)^{1/2}}(1+bb_i(1+x^2)^{1/2})\right]^2 = z^2K_0^2((z^2+b^2b_i)^{1/2}) , \tag{23}$$

where $(z=b/V)$. The corresponding contribution to Eq. (14) is reached through[9]

$$\int_{a_\omega}^\infty dbb\, K_0^2(\alpha b) = \frac{a_\omega^2}{2}[K_1^2(\alpha a_\omega) - K_0^2(\alpha a_\omega)] , \tag{24}$$

$$(\alpha_1^2-\alpha_2^2)\int_{a_\omega}^\infty dbb\, K_0(\alpha_1 b)K_0(\alpha_2 b) = -\alpha_1 a_\omega K_1(\alpha_1 a_\omega)K_0(\alpha_2 a_\omega) + \alpha_2 a_\omega K_0(\alpha_1 a_\omega)K_1(\alpha_2 a_\omega) . \tag{25}$$

Putting together the W_1 and W_2 contribution into the right-hand side Eq. (14) finally yields the stopping expression with $X=\omega a_\omega/V$ and $Y_i^2=X^2+b_i^2a_\omega^2$ under the form

$$\left.\frac{dE}{dx}\right|_\omega = -\frac{4n_iZ_iF_\omega e^4}{m_eV^2} I(X) , \tag{26}$$

with

$$\begin{aligned} I(X) = {} & (N-Z)^2XK_0(X)K_1(X) + N^2\sum_{i=1}^3 a_i^2\left[Y_i^{1/2}K_0(Y_i)K_1(Y_i) + \frac{b_i^2a_\omega^2}{2}[K_0^2(Y_i)-K_1^2(Y_i)]\right] \\ & -2(N-Z)N\sum_{i=1}^3 a_i[X(X^2+Y_i^2)K_0(Y_i)K_1(X) - 2Y_iX^2K_1(Y_i)K_0(X)] \\ & +2N^2\{C_1[-K_0(Y_2)K_1(Y_1)(X^2+Y_2^2)Y_1 + K_0(Y_1)K_1(Y_2)(X^2+Y_1^2)Y_2] \\ & \quad +C_2[-K_0(Y_3)K_1(Y_1)(X^2+Y_3^2)Y_1 + K_0(Y_1)K_1(Y_3)(X^2+Y_1^2)Y_3] \\ & \quad +C_3[-K_0(Y_3)K_1(Y_2)(X^2+Y_3^2)Y_2 + K_0(Y_2)K_1(Y_3)(X^2+Y_2^2)Y_3]\} \end{aligned} \tag{27}$$

where

$$C_1 = \frac{a_1a_2}{b_1^2-b_2^2}, \quad C_2 = \frac{a_1a_3}{b_1^2-b_3^2}, \quad C_3 = \frac{a_2a_3}{b_2^2-b_3^2} .$$

It should be appreciated that the effective interaction (1) results in enhanced stopping in accordance with a reduced core electron interaction proportional to $N[1-\Omega_E(r)]$, $\Omega_E(r)$ being a positive definite quantity. Therefore, the sum of terms beyond the first one, in the right-hand side of Eq. (27), brings in an additional positive contribution to the standard pointlike one.[6,7,10]

The usual pointlike limit is recovered with $N\to 0$. It corresponds to the first term on the r.h.s. of Eq. (27). On the other hand, in the opposite neutral limit $Z=N$, we are left with a nonzero contribution $\sim N^2$ due to the finiteness of the charge distribution. It remains up to us to perform the ω summation in the usual fashion with

TABLE II. Stopping numbers L (a.u.) for the projectile-target system Al^{8+}-Al^{3+} as a function of projectile velocity (a.u.).

V	$L_{ext}(V)$	$L_{pt}(V)$	$(L_{ext}-L_{pt})100/L_{ext}$
4	1279.60	1267.80	0.92
6	1546.24	1534.0	0.79
8	1735.07	1722.60	0.71
10	1882.00	1868.40	0.67
12	1999.80	1987.14	0.63
16	2186.53	2173.83	0.58
20	2330.86	2318.13	0.55
26	2500.10	2487.33	0.51
30	2592.22	2579.44	0.49

TABLE III. As in Table II for Al^{3+}-Al^{8+}.

V	$L_{ext}(V)$	$L_{pt}(V)$	$(L_{ext}-L_{pt})/L_{ext}$
4	110.12	89.565	0.186
6	129.71	108.30	0.165
8	143.35	121.57	0.152
10	153.81	131.83	0.143
12	162.30	140.18	0.136
16	175.55	153.31	0.126
20	185.77	163.46	0.120
26	197.73	175.37	0.113
30	204.23	181.85	0.110

TABLE IV. As in Table II for Al^{3+}-Al^{3+}.

V	$L_{ext}(V)$	$L_{pt}(V)$	$(L_{ext}-L_{pt})/L_{ext}$
4	222.93	178.28	0.200
6	262.26	215.71	0.177
8	289.62	242.24	0.163
10	310.57	262.74	0.154
12	327.53	279.44	0.147
16	354.07	305.70	0.136
20	374.52	326.00	0.130
26	398.43	349.80	0.122
30	411.43	362.73	0.118

$$\int_0^\infty d\omega\, g(\omega)=1, \quad F_\omega=g(\omega)d\omega$$
$$N'g(\omega)=\int d\mathbf{r}\,\rho_i(r)\delta(\omega_0(\mathbf{r})-\omega)\ , \tag{28}$$
$$\omega_0(\mathbf{r})=[\omega_{hyd}^2(\mathbf{r})+\omega_p^2(\mathbf{r})]^{1/2}$$
$$\simeq\sqrt{2}\omega_p(\mathbf{r})=\sqrt{2}\left[\frac{4\pi\rho_i(\mathbf{r})e^2}{m}\right]^{1/2}.$$

The last line of Eq. (28) refers to the standard frequency average where $\omega_p(r)$ is the local plasma frequency pertaining to the stopping bound electrons. The required $\rho_i(r)$ may again be treated with an adequate GSZ effective interaction, fulfilling[11]

$$\rho_i(r)=\frac{N'\Omega_E''(r)}{4\pi r}\ , \tag{29}$$

N' bound electrons to the target ion, derived from the Poisson equation applied to Eq. (1).

From Eq. (26) one thus derives the ω average

$$\frac{dE}{dx}=-\frac{4\pi n_i e^4}{m_e V^2}L(V)\ , \tag{30}$$

with

$$L(V)=\int d\mathbf{r}\,\rho_i(r)I\left[\frac{\omega_0(r)a_\omega}{V}\right], \quad a_\omega^2=\frac{\hbar}{2m_e\omega_0(r)}\ , \tag{31}$$

and $\rho_i(r)$ specified with the adequate parameters [Eqs. (3) and (5)] for target ions. Equation (31) is tabulated (see Tables II, III, and IV) for[12] a few projectile–target-ion pairs of interest for particle-driven fusion.[13] The stopping numbers $L(V)$ are respectively displayed as $L_{ext}(V)$ for the whole r.h.s. of Eq. (27), the extended projectile charge distribution contribution, while $L_{pt}(V)$ refers to the first term, i.e., the pointlike limit. The last column in these tables displays the difference between L_{ext} and L_{pt}, which is negligible (Table II) for a highly stripped projectile.

On the other hand (Tables III and IV), substantial discrepancies seem to arise for ions with a small ionicity, which retain most of their core electrons. The noted discrepancy decreases slowly and steadily with projectile velocity V.

We should consider as highly satisfactory the fact that projectile and target-ion structure could be treated in the same fashion.

Higher target temperature effects ($k_B T_e \geq 10$ eV) will be taken up in a forthcoming work.

IV. LOWER IMPACT-PARAMETER CUTOFF

The analytic, impact formulation displayed in Sec. III requires additional investigation of its stability with respect to numerical modifications of the lower cutoff parameter a_ω. Toward this goal, we have given in Tables V and VI the stopping numbers [Eq. (31)] pertaining to cutoff values a_ω, $a_\omega/2$, and $2a_\omega$ for a few projectile-target pairs. The given L values are not changed by more than 10%. Moreover, the relative discrepancies $L_{ext}-L_{pt}$ remain practically independent of the lower cutoff value. These comforting results clearly demonstrate that the present treatment of long-range contributions to the stop-

TABLE V. Variations of short-range cutoff and impact stopping numbers $L_{ext}(V)$ and $L_{pt}(V)$ in terms of the projectile velocity in a.u. for a projectile with an extended charge distribution and with a pointlike one, respectively. The considered projectile-target pair is Cs^{3+}-Al^{3+}.

Cutoff	a_ω		$a_\omega/2$		$2a_\omega$	
V (a.u.)	L_{ext} (a.u.)	L_{pt} (a.u.)	L_{ext} (a.u.)	L_{pt} (a.u.)	L_{ext} (a.u.)	L_{pt} (a.u.)
4	284.54	89.56	306.77	105.57	259.05	73.70
6	310.29	108.29	329.82	124.27	288.52	92.27
8	326.63	121.56	344.867	137.476	306.77	105.57
10	338.52	131.82	356.027	147.68	319.78	115.87
12	347.85	140.17	364.90	156.00	329.82	124.27
16	362.06	153.30	378.60	169.062	344.87	137.47
20	372.76	163.46	389.021	179.18	356.03	147.68
30	391.75	181.84	407.69	197.51	371.55	166.13

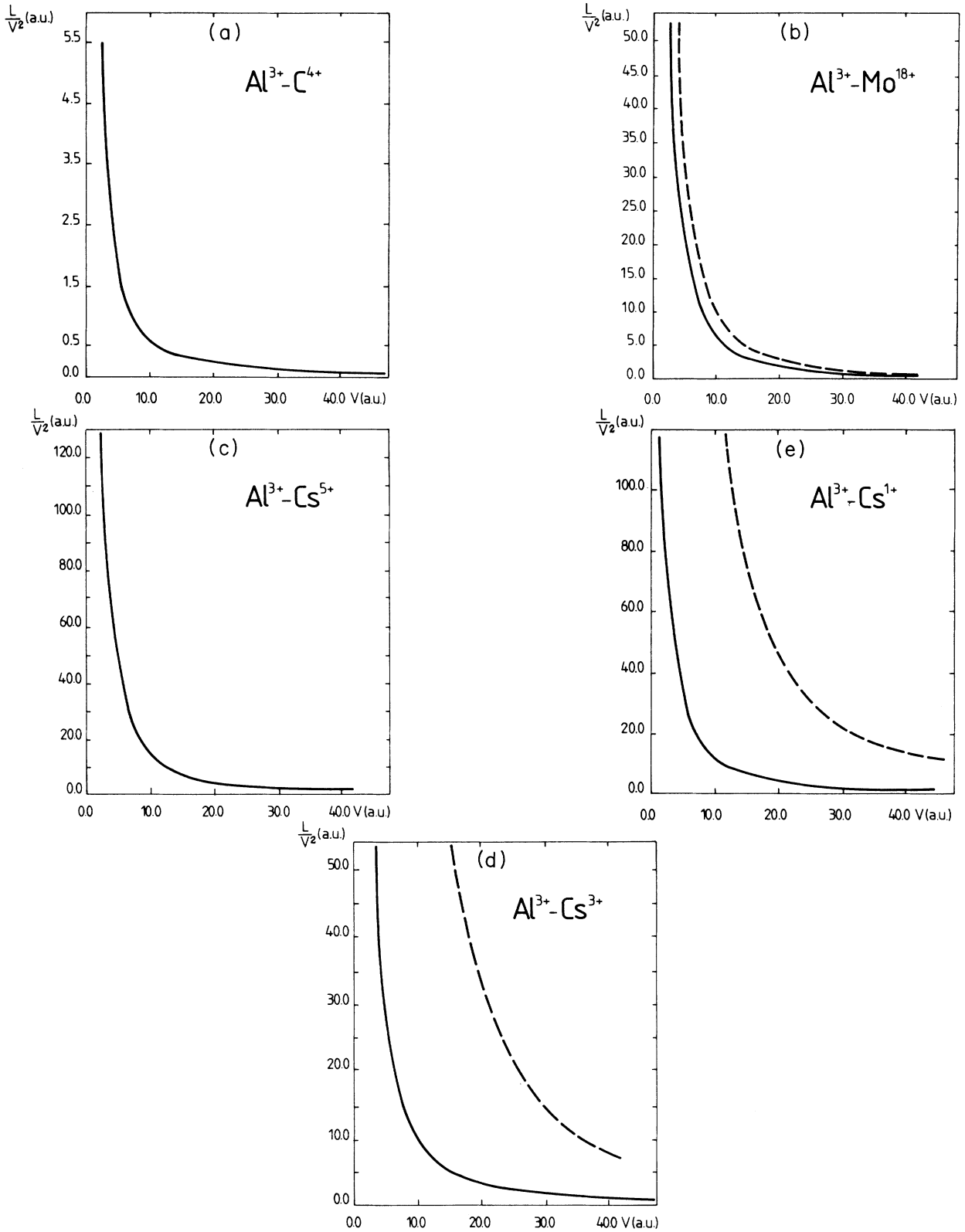

FIG. 2. Stopping powers L/V^2 for Al^{3+} in a dense and partially ionized target made of (a) C^{4+}, (b) Mo^{18+}, (c) Cs^{5+}, (d) Cs^{3+}, and (e) Cs^{+}, in terms of incident velocity V. The dashed upper curve refers to the full Bethe-like stopping expression (26) taking into account the projectile extended structure. The solid curve reproduces the usual pointlike and structureless result arising from restricting the r.h.s. of Eq. (27) to its first term. Note that the ECPE is nearly vanishing in (a) and (b) where the dashed and solid curves overlap strongly.

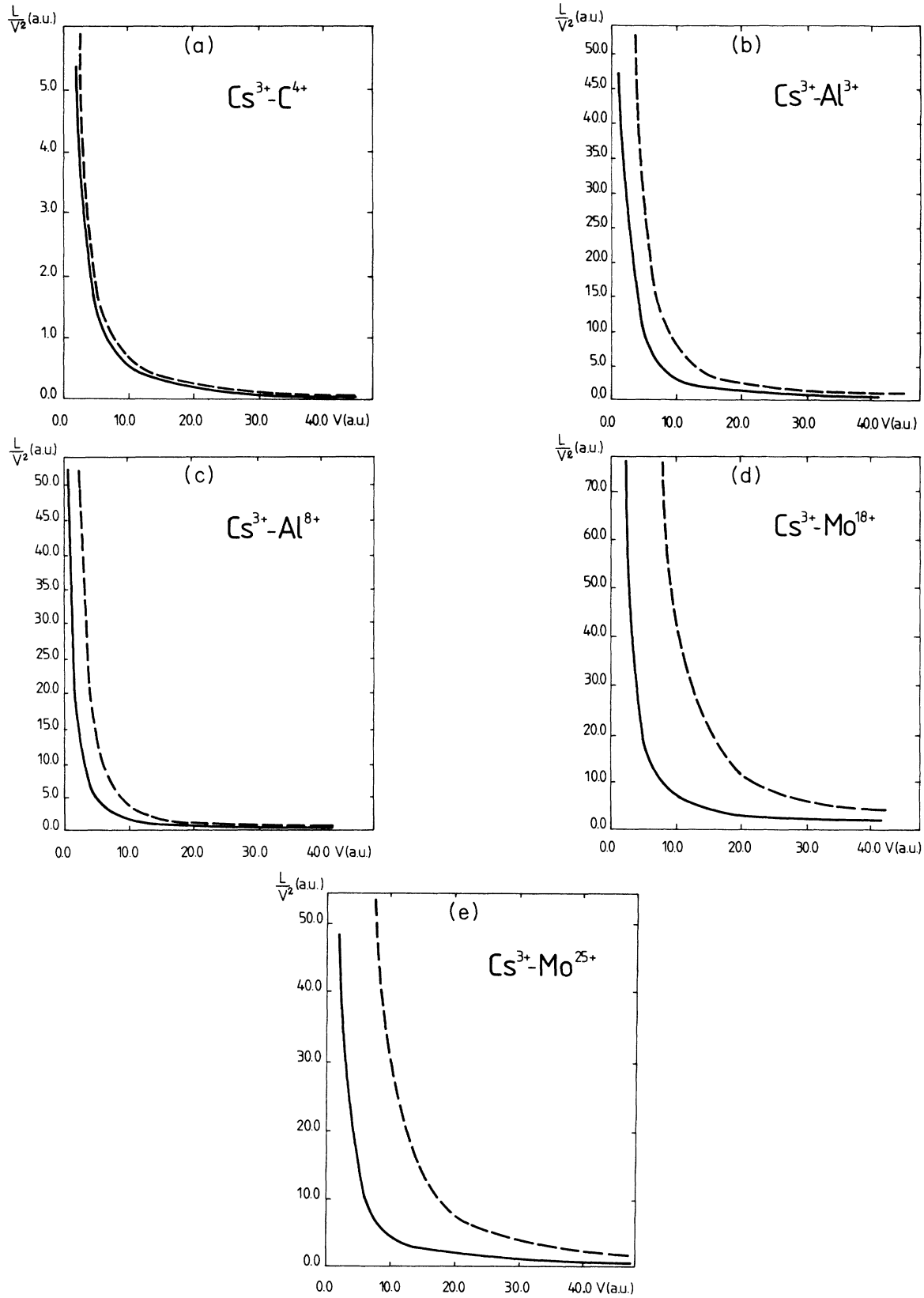

FIG. 3. Stopping powers L/V^2 for Cs^{3+} in a dense and partially ionized target made of (a) C^{4+}, (b) Al^{3+}, (c) Al^{8+}, (d) Mo^{18+}, and (e) Mo^{25+}, in terms of incident projectile velocity. The remainder is the same as in Fig. 2.

TABLE VI. As in Table V for the pair Al^{3+}-Al^{3+}.

Cutoff	a_ω		$a_\omega/2$		$2a_\omega$	
V (a.u.)	L_{ext} (a.u.)	L_{pt} (a.u.)	L_{ext} (a.u.)	L_{pt} (a.u.)	L_{ext} (a.u.)	L_{pt} (a.u.)
4	222.93	178.28	256.61	210.27	188.65	146.6
6	262.26	215.71	295.17	247.66	228.70	183.71
8	289.62	242.24	322.06	274.05	256.61	210.27
10	310.57	262.74	342.71	294.44	277.93	231.00
12	327.53	279.44	359.48	311.05	295.17	247.66
16	354.07	305.70	385.78	337.2	322.06	274.05
20	374.52	326.00	406.08	357.41	342.72	294.41
30	411.43	362	442.82	394.05	380.01	331.1

ping calculation is robust and accurate enough to be taken as a self-consistent one. The remaining task of evaluating the short-range impact contribution will be taken up in a forthcoming work.

V. RESULTS AND DISCUSSION

Equations (26) and (27) are now systematically portrayed in Figs. 2, 3, and 4. We graphed the reduced stopping power L/V^2 in atomic units (a.u.), in terms of the projectile velocity (a.u.). The extended projectile core results pertaining to the full expression (27) lie systematically above their pointlike and structureless homologs given by the first term in the r.h.s. of Eq. (27). The given discrepancy strongly decreases when projectile ionicity increases. A similar trend arises from enhanced target ionization [e.g., Fig. 2(c)]. Quadrature (31) makes it clear that the extended charge distribution of the target ion plays a quantitative role similar to that of the incoming projectile. The target-ion structure is routinely taken care of in many recent calculations.[6,7] This explains why we focus emphasis on the projectile. If we consider a given A-B projectile–target-ion pair, one witnesses the approximate relationship

$$\frac{dE(A\text{-}B)}{dx} \simeq \frac{Z_A^2}{Z_B^2}\frac{dE(B\text{-}A)}{dx} .$$

The extended projectile core effect (EPCE) with its resulting enhanced stopping appears mostly significant for projectile velocity ratios $V/c \leq 0.3$. Therefore the EPCE is likely to be relevant for much of the range of the energetic and intense ion beams envisioned for pellet compression toward achieving the burn of the thermonuclear D+T fuel.

In view of the crucial relevance of the beam-target interactions near the end of the projectile range, it is certainly worthwhile to explore the existence of any EPCE beyond the Bethe-like formulation used in the present work.[13]

It is also to be noted that any quantitative assessment of the EPCE modifications of the usual particle-driven scenarios for inertial confinement fusion should require a full numerical code simulation. The considered enhanced stopping is likely to be strongly correlated to an increased ionization which can markedly reduce the EPCE for many projectile-target pairs. The present results are derived within a general Thomas-Fermi-like (TF) framework for the ion structures (Sec. II) considered as melted, with no shell organization.

The considered GSZ potentials are extrapolated to few-electron systems such as C^{4+}. Despite those simplifications, we expect the present modeling to exhibit the basic trends of the EPCE, especially for heavy ions for which a Thomas-Fermi-like picture becomes increasingly accurate for a larger number of core electrons. As a rule of thumb, we have witnessed that a non-negligible ($\geq 5\%$) EPCE demands that within a given projectile–target-ion pair, one of the partner ionicities remains smaller than 5. Also, the given EPCE is the larger when the two ionicities within the considered projectile–target-ion pair are the smaller. It should be pointed out that the present stopping calculations are

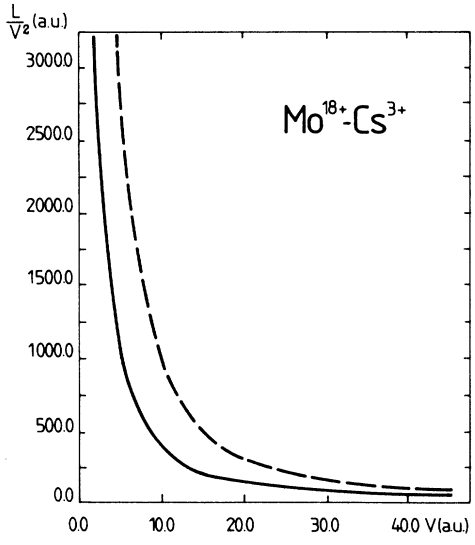

FIG. 4. As in Fig. 2 for the ion projectile Mo^{18+} stopped in a dense and cold plasma ($k_B T \leq 10$ eV) made of partially stripped Cs^{3+} ions.

performed at fixed projectile velocity.

Finally one may notice that the EPCE provides one more enhanced stopping contribution, which is present all along on the projectile trajectory in target, and not especially concentrated near the end of the range.

ACKNOWLEDGMENTS

The Laboratoire de Physique des Gaz et des Plasmas is "Unite Associé au Centre National de la Recherche Scientifique No. 73."

[1]X. Garbet, C. Deutsch, and G. Maynard, J. Appl. Phys. **61**, 907 (1987).

[2]See, for instance, C. Deutsch, G. Maynard, and H. Minoo, in *Laser Interaction and Related Plasma Phenomena,* edited by H. Hora (Plenum, New York, 1984), Vol. 6, p. 1029; C. Deutsch, Ann. Phys. (Paris) **11**, 1 (1986).

[3]Y. K. Kim and K. T. Cheng, Phys. Rev. A **22**, 61 (1980), and references contained therein.

[4]R. H. Garvey and A. E. S. Green, Phys. Rev. A **13**, 931 (1976).

[5]R. H. Garvey, C. H. Jackman, and A. E. S. Green, Phys. Rev. A **12**, 1144 (1975).

[6]J. C. Ashley, R. H. Ritchie, and W. Brandt, Phys. Rev. B **5**, 2393 (1972).

[7]J. D. Jackson and R. L. McCarthy, Phys. Rev. B **6**, 4131 (1972).

[8]G. Maynard and C. Deutsch, J. Phys. (Paris) **43**, L223 (1982).

[9]*Tables of Integral Transforms,* edited by A. Erdelyi (McGraw-Hill, New York, 1953), Vol. 1.

[10]J. D. Jackson, *Classical Electrodynamics* (Wiley, New York, 1975), p. 623.

[11]A. E. S. Green, D. L. Sellin, and A. S. Zachor, Phys. Rev. **181**, 1 (1969).

[12]A survey of this section already appeared in C. Deutsch and G. Maynard, Europhys. Lett. **7**, 31 (1988).

[13]C. Deutsch, P. Fromy, X. Garbet, and G. Maynard, Fusion Technol. **13**, 362 (1988).